Nonlinear Adaptive Flight Control for the X-38 Vehicle

Elmar M. Wallner and Klaus H. Well
Institute of Flight Mechanics and Control
University of Stuttgart
Pfaffenwaldring 7a, 70569 Stuttgart, Germany
klaus.well@ifr.uni-stuttgart.de

***Abstract* - The paper is concerned with designing an attitude control system for the X-38 vehicle for the hypersonic and supersonic region. The design goals are i) good tracking performance such that the vehicle will follow the guidance commands, ii) robust stability and performance in view of uncertain aerodynamic parameters, iii) cross-airframe capability of the control architecture in order to minimize redesign efforts in view of vehicle modifications which might occur during the development process. These goals have been achieved by selecting an inversion based control system design procedure combined with a CMAC neural net for adaptation of the linear PID controller parameters in view of the uncertainties. It is shown that the application of dynamic inversion requires a redefinition of the controlled variables in order to adequately stabilize the closed-loop system. The need for output-redefinition lies in the fact that only two bodyflaps are available for control, which limits the number of controlled variables to two. Simulation results are given to show the efficacy of the control approach.**

I Introduction

In the past, attitude control of reentry vehicles was based primarily on gain-scheduled classical controllers. For future reentry vehicles as for instance the X-38 - whose further development has been canceled in the meantime - new concepts for control system design have been under investigation. The authors have been fortunate to have had access to a complete database of that vehicle and, therefore, have taken that vehicle as the reference vehicle for the present paper. The approach considered is definitely applicable to similar vehicles, lets say to all winged or lifting body vehicles with a maximum L/D in the hypersonic region of more than 0.5. The approach considered is that of feedback linearization, also referred to as dynamic inversion (DI), supplemented by a neural network in order to robustify the design. This approach offers the following advantages:

- (almost) no gain scheduling of the controller,
- in-flight controller adaptation leading to compensation of large modelling errors,
- flexible cross-airframe adaptability of the controller.

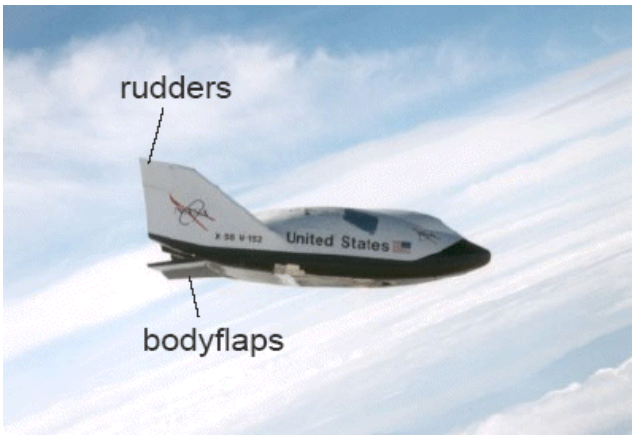

Fig. 1: The X-38 vehicle and its actuators

In a previous paper [1] a DI controller was presented utilizing a time scale separation between the attitude dynamics and the attitude-rate dynamics. This design was based on the assumption that actuators are available for generating moments about all three body axes. However, this assumption is only valid in certain regions of the flight envelope of a reentry vehicle. If, for instance, only body flaps can be used for attitude control the design problem becomes more intricate in the sense that internal dynamics are present. This has been addressed in [2]. One of the drawbacks of DI has been in the past the lack of robustness of the closed loop system since the design is based on some knowledge of the vehicle dynamics. In order to deal with that issue the controller gains may be adapted by either applying methods of classical robust control system designs such as f.i. H_∞ or - as is being presented in this paper - by using a neural network [3], [4].

II The X-38 Vehicle

The reentry trajectory of the X-38 can be subdivided into several phases where each phase is characterized by engaging a different set of control effectors. It is for this reason that the X- 38 does not permit the realization of a single DI controller to cover the complete reentry. Attitude control of a reentry vehicle usually demands decoupled control of three attitude angles. A necessary condition for this is that the

vehicle possesses at least three control inputs. This is satisfied by the X-38 configuration only in the early and late phases of reentry, where either rudders or the RCS can be employed in support of the bodyflaps. In these phases the design using DI is rather straightforward. It is based on the assumption of a time scale separation between attitude angles and attitude rates, [4] and [11]. During a significant portion of the flight, attitude control has to be accomplished using only the two bodyflaps, see Fig. 2. As is shown in the following, decoupled control is unfeasible, regardless of the control method used.

III The Equations of Motion

The complete state vector for the nonlinear motion consists of $(\lambda, \tau, h, V, \gamma, \chi, \alpha, \beta, \mu, p, q, r)$, where the first three components describe the position of the vehicle, the second three the air-path velocity, path inclination, and azimuth in a flight path coordinate system, the next three the attitude (angle of attack, sideslip angle, and velocity bank angle), and the last three angular velocities about the body fixed axes. For attitude control system design the last six components of the state vector are of interest, only. The equations of motion for these six states are

$$\dot{\alpha} = q - \tan\beta(p\cos\alpha + r\sin\alpha) - \frac{(F^L - mg\cos\gamma\cos\mu)}{mV\cos\beta} \quad (1)$$

$$\dot{\beta} = p\sin\alpha - r\cos\alpha + \frac{1}{mV}(-Y + mgcos\gamma\sin\mu) \quad (2)$$

$$\dot{\mu} = \frac{1}{\cos\beta}(p\cos\alpha + r\sin\alpha) + \frac{\tan\beta}{mV}(F^L - mg\cos\gamma\sin\mu) + \frac{\tan\gamma}{mV}(F^L\sin\mu - Y\cos\mu) \quad (3)$$

$$\dot{p} = \frac{I_{zz}L + I_{xz}N + pqI_{xz}(I_{zz} + I_{xx} - I_{yy})}{I_{xx}I_{zz} - I_{xz}^2} + \frac{qr(I_{zz}(I_{yy} - I_{zz}) - I_{xz}^2)}{I_{xx}I_{zz} - I_{xz}^2} \quad (4)$$

$$\dot{q} = \frac{M + (I_{zz} - I_{xx})pr + I_{xz}(r^2 - p^2)}{I_{yy}} \quad (5)$$

$$\dot{r} = \frac{I_{xz}L + I_{xx}N + pq(I_{xz}^2 + I_{xx}(I_{xx} - I_{yy}))}{I_{xx}I_{zz} - I_{xz}^2} + \frac{qrI_{xt}(I_{yy} - (I_{xx} - I_{zz}))}{I_{xx}I_{zz} - I_{xz}^2} \quad (6)$$

F^L is the aerodynamic lift force, mg the weight, Y the side force, I_{ij} the moments of inertia about the ij axes. M, L, N are the external moments about the body x, y, z -axes.

As will become apparent later on it is necessary to consider the aerodynamic moments in a linear approximation around some trimmed condition. This can be formulated as

$$\begin{bmatrix} L \\ M \\ N \end{bmatrix} = \begin{bmatrix} L_{\delta a}\delta_a + L_\beta\beta \\ M_{\delta e}(\delta_e - \delta_{eT}) + M_\alpha(\alpha - \alpha_T) \\ N_{\delta a}\delta_a + N_\beta\beta \end{bmatrix}. \quad (7)$$

Here, the subsripted moments are the partial derivatives with respect to elevator and aileron deflections δ_e, δ_a and angle of attack and sideslip angle. The subscript T refers to a trimmed condition.

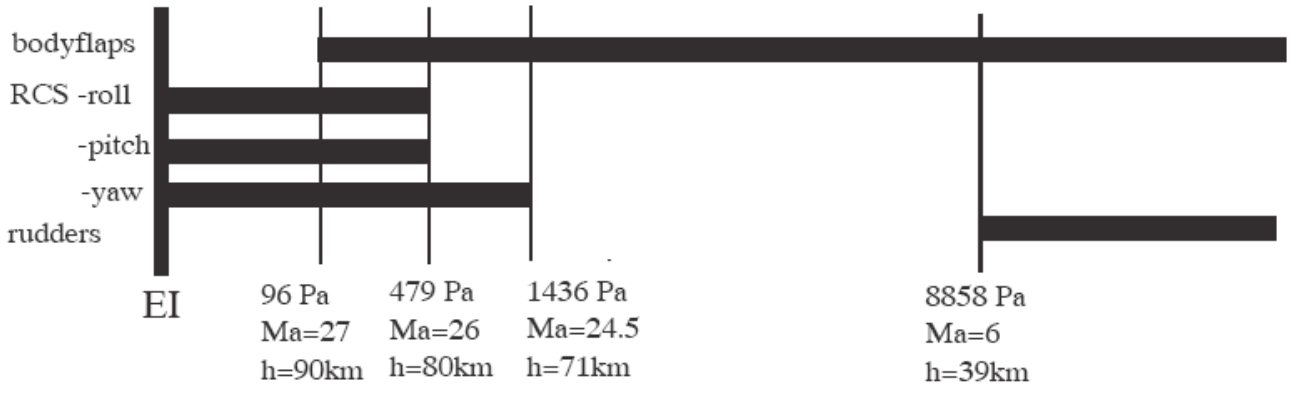

Fig. 2: Permitted actuator utilization

In addition, it will become necessary to linearize the lift- and side force as

$$\begin{bmatrix} F^L \\ Y \end{bmatrix} = \begin{bmatrix} F_T^L + F_\alpha^L(\alpha - \alpha_T) \\ Y_\beta \beta \end{bmatrix}. \tag{8}$$

The equations of motion can be linearized along some nominal reference trajectory and the poles are plotted in Fig. 3 for a nominal reentry with an interval of 2.5 km of flight altitude. The arrows indicate the general movement of the poles. In the longitudinal motion we can identify a typical short period mode, a long period phugoid mode and a real pole corresponding to the altitude mode.

The movement of the short period mode poles is particularly interesting with regard to attitude control. Obviously, the mode is only slightly damped. In order to adequately stabilize the system and ensure satisfactory performance over the whole reentry, measures need to be taken to adapt the controller to flight condition. Gain scheduled control is a possibility to that end. The lateral motion is characterized by a dutch roll mode as well as roll and spiral modes. Similar to the short period mode, the dutch roll varies strongly with flight condition and is only slightly damped. Note that the roll and spiral modes cannot be clearly distinguished over the whole reentry. At some flight conditions, the two corresponding real poles merge to form a single oscillatory mode, the so-called lateral phugoid. This mode is known to occur for lifting body configurations.

IV The Affine Form of the EOM and the Normal Form

By substituting the expressions for L,M,N in (4)-(6) with (7) the equations of motion become linear in the controls and may be cast in the form

$$\dot{x} = f(x) + G(x)u \tag{9}$$

with f as 6-vector containing the state dependence of the right hand sides of (1)-(6) and $G = \begin{bmatrix} g_1 & g_2 \end{bmatrix}$ where

$$g_1 = \begin{bmatrix} 0 \\ 0 \\ 0 \\ 0 \\ M'_{\delta e} \\ 0 \end{bmatrix}, \; g_2 = \begin{bmatrix} 0 \\ 0 \\ 0 \\ L'_{\delta a} \\ 0 \\ N'_{\delta a} \end{bmatrix} \text{ and } u = \begin{bmatrix} \delta_e \\ \delta_a \end{bmatrix}, \tag{10}$$

with

$$L'_{\delta a} = \frac{I_{zz} L_{\delta a} + I_{xz} N_{\delta a}}{I_{xx} I_{zz} - I_{xz}^2}, \; N'_{\delta a} = \frac{I_{xz} L_{\delta a} + I_{xx} N_{\delta a}}{I_{xx} I_{zz} - I_{xz}^2}, \tag{11}$$

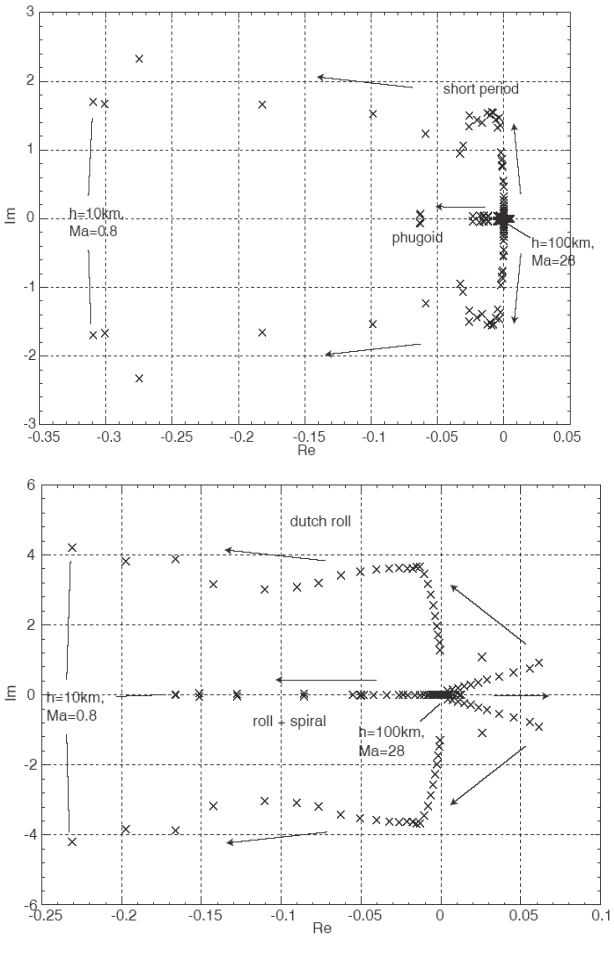

Fig. 3: Poles of longitudinal (top) and lateral (bottom) motion

$$M'_{\delta e} = \frac{M_{\delta e}}{I_{yy}}. \tag{12}$$

The output equation for the case that rudder can not be used becomes

$$y = h(x) \text{ with } h = \begin{bmatrix} h_1 & h_2 \end{bmatrix}, \tag{13}$$

$$h_1 = \alpha - \alpha_T = \Delta\alpha, \; h_2 = \mu, \tag{14}$$

that is in a first attempt the controller is conjectured to track angle of attack and velocity bank angle.

In order to proceed with the development of a DI controller the normal form of the equations of motion is needed. To this end the relative degree of the output must be determined. By inspection of (1)-(6) one easily sees that the relative degree for both outputs is 2 each. This gives a vector relative degree

of 4 and thus indicates that there will exist some internal dynamics.

To build the normal form a mapping Φ of $x \to (\xi, \eta)$ must be defined where ξ, η are the external and internal states of the normal form. According to [5], [6] this is done by making use of the Lie derivatives of the output. The Lie derivatives needed here are

$$L_f h_i(x) = \frac{\partial h_i}{\partial x}(x) f(x),$$
$$L_f^2 h_i(x) = \frac{\partial}{\partial x}(L_f h_i) f(x), \; i = 1, 2, \tag{15}$$

and

$$L_{g_j} L_f h_i(x) = \frac{\partial}{\partial x}(L_f h_i) g_j(x), \; \{i,j\} \in \{1,2\}. \tag{16}$$

Using these definitions one obtains the mapping

$$\begin{aligned} \Phi_1 &= h_1(x) = \Delta\alpha \\ \Phi_2 &= L_f h_1(x) = f_1(x) \\ \Phi_3 &= h_2(x) = \mu \\ \Phi_4 &= L_f h_2(x) = f_3(x) \end{aligned} \tag{17}$$

From the additional conditions

$$L_{g_2} \Phi_5 = L_{g_2} \Phi_6 = 0 \tag{18}$$

one obtains furthermore

$$\Phi_5 = \beta \tag{19}$$
$$\Phi_6 = \frac{p}{L'_{\delta a}} - \frac{r}{N'_{\delta a}}$$

Thus, the normal external and internal states are

$$\begin{bmatrix} \xi_1 \\ \xi_2 \\ \xi_3 \\ \xi_4 \end{bmatrix} = \begin{bmatrix} \Delta\alpha \\ f_1 \\ \mu \\ f_3 \end{bmatrix}, \begin{bmatrix} \eta_1 \\ \eta_2 \end{bmatrix} = \begin{bmatrix} \beta \\ \dfrac{p}{L'_{\delta a}} - \dfrac{r}{N'_{\delta a}} \end{bmatrix}. \tag{20}$$

The internal dynamics are

$$\begin{bmatrix} \dot{\eta}_1 \\ \dot{\eta}_2 \end{bmatrix} = \begin{bmatrix} f_2 \\ \dfrac{f_4}{L'_{\delta a}} - \dfrac{f_6}{N'_{\delta a}} \end{bmatrix}. \tag{21}$$

Condition (18) and the state transformation (19) lead to a formulation of the internal dynamics in (21) which is independent of the controls. This facilitates the control design later on. In order to analyze the stability properties of the

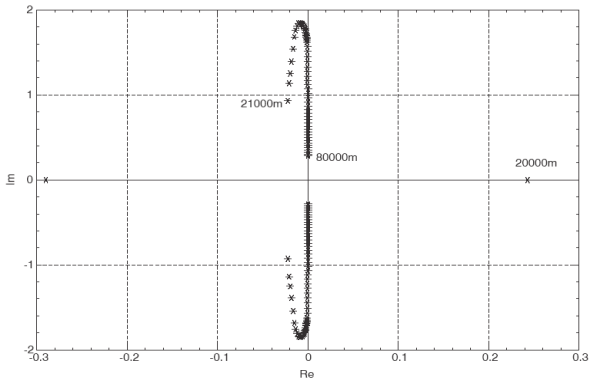

Fig. 4: Poles of the zero-dynamics

internal dynamics one needs to linearize (21) around the origin. This leads to

$$J_{\eta 11} = -\frac{Y_\beta}{mV}, \ldots J_{\eta 12} = \frac{L'_{\delta a} N'_{\delta a}}{L'_{\delta a} \cos\alpha_T + N'_{\delta a} \sin\alpha_T} \tag{22}$$
$$J_{\eta 21} = \frac{N'_{\delta a}(I_{zz} L_\beta + I_{xz} N_\beta) - L'_{\delta a}(I_{xz} L_\beta + I_{xx} N_\beta)}{L'_{\delta a} N'_{\delta a}(I_{xx} I_{zz} - I_{xz}^2)}$$
$$I_{\eta 22} = 0$$

Fig. 4 (numbers indicate altitude for a nominal reentry trajectory) shows that the zero-dynamics is almost completely undamped for higher altitudes and becomes unstable for lower altitudes.

V The DI Controller Design

If one proceeds with the development of a DI controller despite this fact the design equations for the controller are

$$\begin{bmatrix} \dot{\xi}_2 \\ \dot{\xi}_4 \end{bmatrix} = b(x) + A(x) u, \; u = \begin{bmatrix} \delta_e \\ \delta_a \end{bmatrix}. \tag{23}$$

The elements of the control distribution matrix A are obtained from

$$a_{11} = L_{g_1} L_f^1 h_1 = \frac{\partial f_1}{\partial x} g_1 = M'_{\delta_e} \tag{24}$$
$$a_{12} = L_{g_2} L_f^1 h_1 = \frac{\partial f_1}{\partial x} g_2 = -\tan\beta(\cos\alpha L'_{\delta a} + \sin\alpha N'_{\delta a})$$
$$a_{21} = 0$$
$$a_{22} = L_{g_2} L_f^1 h_2 = \frac{\partial f_3}{\partial x} g_2 = \frac{1}{\cos\beta}(\cos\alpha L'_{\delta a} + \sin\alpha N'_{\delta a})$$

$$b_1 = L_f\Phi_2 = \frac{\partial\Phi_2}{\partial x}f \quad . \tag{25}$$
$$b_2 = L_f\Phi_4 = \frac{\partial\Phi_4}{\partial x}f$$

These two terms are not given explicitly since they are rather lengthy. Then u is obtained from

$$u = A^{-1}(b - \nu) \tag{26}$$

with ν as pseudocontrol and

$$A^{-1} = \begin{bmatrix} \dfrac{1}{M'_{\delta e}} & \dfrac{\sin\beta}{M'_{\delta e}} \\ 0 & \dfrac{\cos\beta}{\cos\alpha L'_{\delta a} + \sin\alpha N'_{\delta a}} \end{bmatrix}. \tag{27}$$

On order to design the linear controller for ν one needs to look at the error dynamics of the closed loop system. Remember that a tracking controller for $h_1 = \Delta\alpha$ and $h_2 = \mu$ is desired. The tracking error can be defined as

$$e = \begin{bmatrix} e_1 \\ e_2 \end{bmatrix} = h - h_c = \begin{bmatrix} h_1 - h_{1c} \\ h_2 - h_{2c} \end{bmatrix} \tag{28}$$

where the subscript c indicates commanded value. One may define a filtered tracking error

$$r = \dot{e} - \bar{\Lambda}e \text{ with } \bar{\Lambda} = \begin{bmatrix} \bar{\lambda}_1 & 0 \\ 0 & \bar{\lambda}_2 \end{bmatrix} \tag{29}$$

as user choosable constants. The error dynamics then are

$$\dot{r} = \nu - \ddot{h}_c + \bar{\Lambda}\dot{e}\,. \tag{30}$$

The choice of

$$\nu = \ddot{h}_c - \bar{\Lambda}\dot{e} - Kr\,,\; K = \begin{bmatrix} k_1 & 0 \\ 0 & k_2 \end{bmatrix} \tag{31}$$

ensures asymptotic decay of the filtered tracking error for a proper choice of K.

The pseudocontrol needs first and second derivatives of the commanded values. These can be generated by filtering the commands through a second order filter of the form

$$G_m = \frac{\omega_m^2}{s^2 + 2\zeta_m\omega_m s + \omega_m^2} I_{2\times 2} \tag{32}$$

where ζ_m, ω_m are damping and frequency of a suitable model behavior and $I_{2\times 2}$ is an identity matrix.

Using this design, nonlinear simulations are performed for two initial conditions. The first simulation is conducted for an initial altitude of 60km (Ma = 18.5). As is to be seen from Fig. 5, the angle of attack and bank angle follow the respective reference signals (dashed lines) quite closely. Small oscillations are to be observed in bank angle which the controller fails to fully attenuate. Apparently, the maneuver excites the internal system dynamics which results in a nearly undamped, though bounded, oscillation in sideslip angle. This behavior was implicated by the locations of the poles of the zero-dynamics. Obviously, this tracking behavior is unacceptable as the oscillations would entail energy consuming actuator activity, detrimental side heating of the vehicle, degraded flight performance and passenger discomfort. The second simulation is performed at an initial altitude of 20km (Ma=1.7). Due to the fact that the system at these conditions is non-minimum phase the vehicle departs after only 13 sec. The mechanism behind this instability can be interpreted as follows. If a disturbance causes the controller to correct the bank angle, then an aileron deflection is commanded which counters the disturbance. However, due to large adverse yaw of the ailerons in conjunction with the lack of directional stability, the vehicle initiates a yaw divergence which causes a build-up of sideslip angle. The sideslip, in turn, induces a roll moment opposed to the roll moment generated by the ailerons. This causes a larger aileron deflection and the divergence is aggravated. Eventually, the boldfaces attain their maximum deflection and the roll moment due to sideslip exceeds

the aileron roll moment, causing the vehicle to depart in roll. The rolling motion is opposite to the direction insinuated by the aileron deflection, hence the designation “aileron reversal”. Likewise, the position saturation of the boldfaces causes a divergence in the longitudinal motion.

VI Stabilizing the Internal Dynamics

From the above simulation it obvious that the unacceptable dynamic behavior is primarily associated with the lateral motion. This motion is influenced by the second tracking command h_{2c}. Following the procedure suggested in [7] and [8] this output is redefined. To this end, in a first step, the relative degree is reduced to 1 in that output. As a result, the original output variables become state variables of the ensuing internal dynamics. In the second step, the output is redefined in such a way that the zerodynamics are (locally) stabilized. A corresponding redefined desired output ensures that adequate tracking performance in the original output variable is retained. The new output is chosen to be

$$h_2 = \dot{\mu} + \kappa\mu - \bar{k}_1\mu - \bar{k}_2\beta - \bar{k}_3\left(\frac{p}{L'_{\delta a}} - \frac{r}{N'_{\delta a}}\right) \tag{33}$$

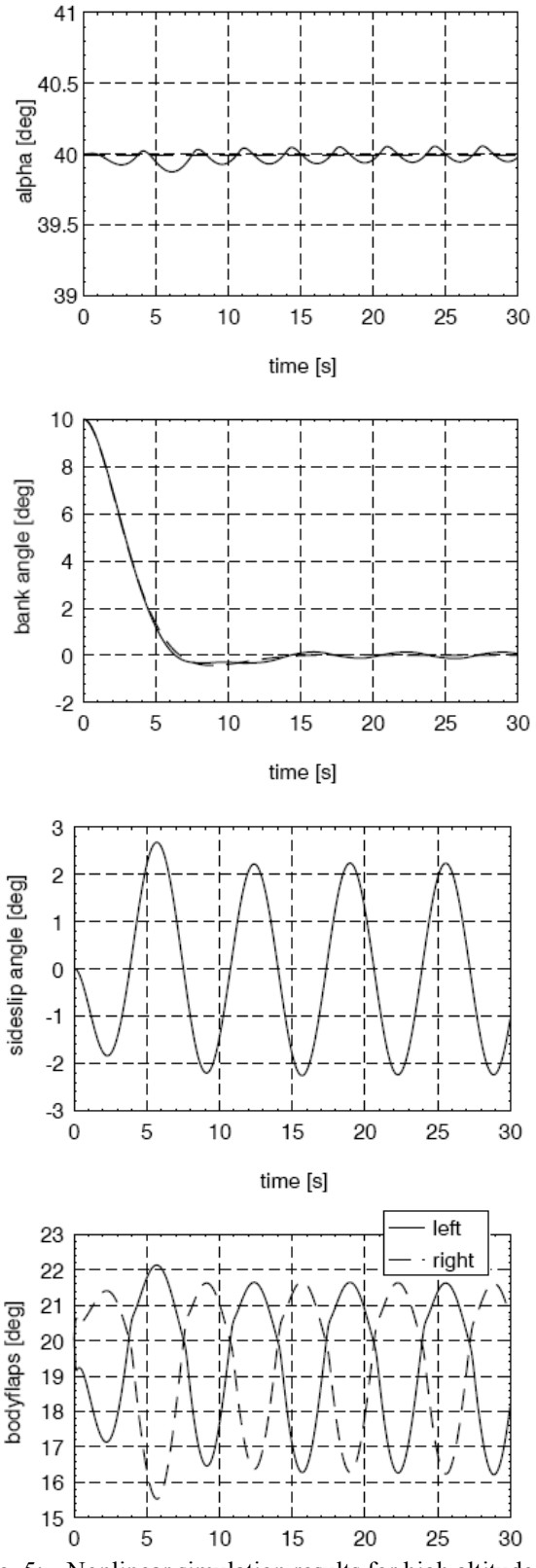

Fig. 5: Nonlinear simulation results for high altitude

with $\bar{k}_1, \bar{k}_2, \bar{k}_3$ appropriately chosen constants. The mapping Φ_3 then becomes

$$\Phi_3 = f_3(x) + \kappa\mu - \bar{k}_1\mu - \bar{k}_2\beta - \bar{k}_3\left(\frac{p}{L'_{\delta a}} - \frac{r}{N'_{\delta a}}\right) \qquad (34)$$

and the new external and internal states are

$$\begin{bmatrix}\xi_1\\ \xi_2\\ \xi_3\end{bmatrix} = \begin{bmatrix}\Delta\alpha\\ f_1\\ f_3(x) + (\kappa - \bar{k}_1)\mu - \bar{k}_2\beta - \bar{k}_3\left(\frac{p}{L'_{\delta a}} - \frac{r}{N'_{\delta a}}\right)\end{bmatrix},$$

$$\begin{bmatrix}\eta_1\\ \eta_2\\ \eta_3\end{bmatrix} = \begin{bmatrix}\mu\\ \beta\\ \frac{p}{L'_{\delta a}} - \frac{r}{N'_{\delta a}}\end{bmatrix}. \qquad (35)$$

Linearizing the internal dynamics in the same way as was described previously one can analyze the poles and select the constants in (34) such that desired stability properties are ensured along a typical reentry trajectory. Here, it is chosen to schedule the parameters as function of Machnumber such that sensitivity of the poles is minimized with respect to uncertainties in the model parameters $L'_{\delta a}, N'_{\delta a}, L_\beta, N_\beta$, [2].

VII Adaptation in the Presence of Uncertainty

The DI controller design needs a model of the dynamics. In reality, however, the model parameters are uncertain. This uncertainty can be expressed, for instance, in equations (23) by assuming

$$\hat{b} + \hat{A}u = b + Au + \Delta_m(x, u), \qquad (36)$$

the hat indicating the real dynamics while the unmarked

.

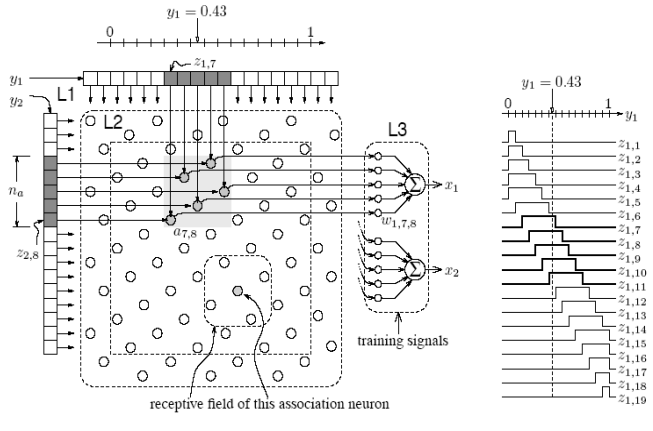

Fig. 6: Principal architecture of a CMAC neural net

variables indicate the design equations. The pseudocontrol is then appended by

$$\nu = \nu_o + \nu_{ad} + \nu_b . \tag{37}$$

ν_o is the control without uncertainty, for instance as given in (31). ν_{ad} and ν_b are computed using a Cerebellar Model Articulation Controller (CMAC) as described in [9] and [10]. The basic operation of a two-input two-output CMAC network is illustrated in Fig. 6 (taken with permission from [10]). It has three layers, labeled L1, L2, L3 in the figure. The inputs are the values y_1 and y_2. Layer 1 contains an array of "feature detecting" neurons z_{ij} for each input y_i. Each of these outputs one for inputs in a limited range, otherwise they output zero (right side of Figure). For any input y_i a fixed number of neurons (na) in each layer 1 array will be activated (na = 5 in the example). The layer 1 neurons effectively quantize the inputs. Layer 2 contains n_v association neurons a_{ij} which are connected to one neuron from each layer 1 input array z_{1i}, z_{2j}. Each layer 2 neuron outputs 1.0 when all its inputs are nonzero, otherwise it outputs zero—these neurons compute the logical AND of their inputs. They are arranged so exactly na are activated by any input (5 in the example). Layer 3 contains the n_x output neurons, each of which computes a weighted sum of all layer 2 outputs, i.e.:

$$x_i = \sum_{jk} w_{ijk} a_{ik} . \tag{38}$$

The parameters w_{ijk} are the weights which parameterize the CMAC mapping (w_{ijk} connects a_{jk} to output i). There are n_x weights for every layer 2 association neuron, which makes $n_v \times n_x$ weights in total. Only a fraction of all the possible association neurons are used. They are distributed in a pattern which conserves weight parameters without degrading the local generalization properties too much. Each layer 2 neuron has a receptive field that is $n_a \times n_a$ units in size, i.e. this is the size of the input space region that activates the neuron. The CMAC was intended by Albus to be a simple model of the cerebellum. It has been selected here because of its implementation speed.

By approximating Δx in (31) with

$$\Delta x = W^T \Gamma(x) , \tag{39}$$

where Γ is a vector containing all outputs coming out of layer 2, say length N_a, and W is an $N_a \times m$ matrix consisting of all weights w_{ijk}, adaptation is achieved by

$$\nu_{ad} = -W^T \Gamma(x) . \tag{40}$$

The weights are obtained from the online computation of

$$\dot{W} = \beta[\Gamma r^T - \sigma_w \|r\| M_\Gamma W] . \tag{41}$$

Here, β is the adaption rate of the network. r is the filtered tracking error as in (29), σ_w is a design parameter in order to prevent a parameter drift. M_Γ is a diagonal matrix which contains all elements of the layer 2 which are active either 1 or 0 depending on whether a particular element in L2 is active or not. Initially, all elements of W are zero.

The third term in the right hand side of (37) is to compensate for neural net approximation errors. It is defined as

$$\nu_b = \phi \psi , \tag{42}$$

where

$$\phi = \begin{bmatrix} \tanh\left(\frac{r_1}{\delta_1}\right) & 0 \\ 0 & \tanh\left(\frac{r_2}{\delta_2}\right) \end{bmatrix} \tag{43}$$

in our application. δ_1, δ_2 being some design parameter. $\psi = \begin{bmatrix} \psi_1 & \psi_2 \end{bmatrix}^T$ is obtained from

$$\dot{\psi} = \gamma \left[\begin{bmatrix} r_1 & 0 \\ 0 & r_2 \end{bmatrix} \psi - \sigma_\psi \|r\| (\psi - \psi_0) \right] . \tag{44}$$

Here, γ is an adaption rate parameter, again, σ_ψ ensures boundedness, and ψ_0 is a constant design parameter as well. It is shown in [11] that using (40)-(44) both the elements of W and ψ remain bounded as long as their initial values are smaller $1/\sigma_w$ or $1/\sigma_\psi$ respectively.

VIII Nonlinear Simulation Results

The adaptive control for the redefined output in section V is obtained from

$$\nu_0 = \begin{bmatrix} \ddot{h}_{1c} - k_1 r_1 + -\bar{\lambda}_1 \dot{e}_1 \\ \dot{h}_{2c} - k_2 r_2 \end{bmatrix} , \tag{45}$$

ν_{ad}, ν_b as described in section VI. The controller parameters are selected as

$$\begin{aligned} &k_1 = 2, k_2 = 2, \bar{\lambda}_1 = 1, \beta = 30, \psi_{i0} = 30, \gamma = 1 \\ &\delta_i = 1, \sigma_w = \sigma_\psi = 0{,}01 \end{aligned} \tag{46}$$

Fig. 7 shows the results for a large portion of the reference trajectory. This simulation is conducted under significant aerodynamic model uncertainties. It commences at an initial altitude of 62 km (Ma = 20.0) and terminates at 31 km altitude and a Mach number of Ma = 4.3. It exhibits two large bank reversals. In the middle figure the pseudocontrols are depicted. In the lower figure the activated receptors of the

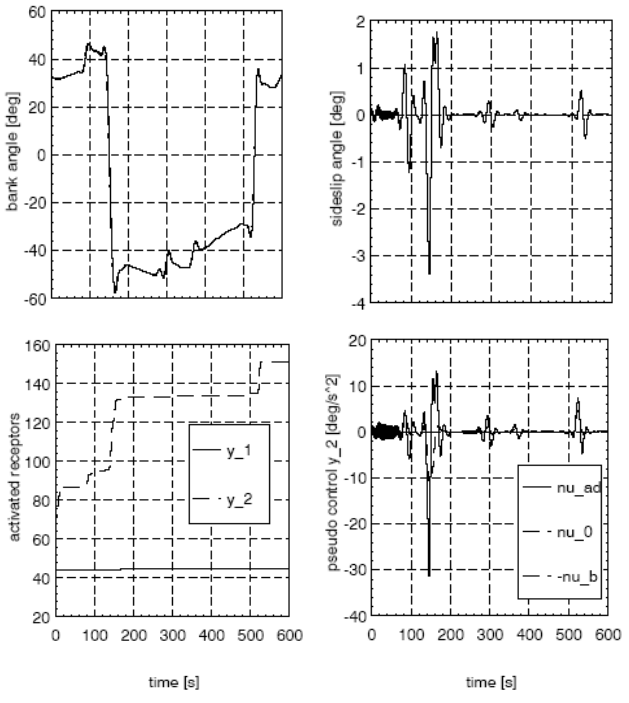

Fig. 7: Nonlinear simulation results with stabilized internal dynamics and adaptation

CMAC net are given. It is obvious that at the time of the bank reversals the net is activated in particular.

The adaptation rates are selected on the basis of simulations. Since the control concept does not account for unmodelled dynamics, care is taken so that these are not excited by excessive adaptation rates. To that end, the adaptation rates are chosen well below the critical values, which were found to impair robustness to high frequency unmodelled dynamics, particularly actuator dynamics. The baseline controller gains are selected so as to ensure satisfactory nominal tracking performance. The leakage parameters are chosen relatively small so that they do not impair rapid adaptation and tracking performance. No problems regarding parameter drift are observed applying these small parameters. All adaptive parameters are initialized at a value of zero. Nonlinear simulations under considerable uncertainties in the aerodynamic coefficients (up to 50%) show that the considerable tracking errors without adaption are mitigated to a satisfactory level. The controller parameters need no scheduling except for three scalar design parameters which are scheduled with Machnumber.

References

[1] Roenneke, Axel J., Well, Klaus H.: "Nonlinear Flight Control for a High-Lift Reentry Vehicle", *AIAA Guidance, Navigation, and Control Conference*, AIAA 95-3370-CP, Baltimore, Md., 1995, pp. 1798-1805.

[2] Wallner, E., Well, K.H., "Attitude Control of a Reentry Vehicle with Internal Dynamics," *Proceedings of the AIAA Guidance, Navigation, and Control Conference*, AIAA Paper 2002-4647, 2002.

[3] Calise, A.J., Rysdyk, R.T., "Nonlinear Adaptive Flight Control Using Neural Networks",*IEEE Control Systems Magazine*, Vol. 18, No. 6, 1998, pp. 14-25.

[4] Wallner, E., Well, K.H., "Nonlinear Flight Control Design for the X-38 Using CMAC Neural Networks," *Proceedings of the AIAA Guidance, Navigation, and Control Conference*, AIAA Paper 2001-4042, 2001.

[5] Isidori, A.,*Nonlinear Control Systems*, Springer-Verlag, Berlin, 1989.

[6] Allgöwer, F., Näherungsweise Ein-/Ausgangs-Linearisierung nichtlinearer Systeme, *Fortschrittberichte VDI,* Reihe 8 Nr. 582, VDI Verlag, Düsseldorf, 1996.

[7] Gopalswamy, S., Hedrick, J.K., "Tracking Nonlinear Non-Minimum Phase Systems Using Sliding Control," *International Journal of Control,* Vol. 57, No. 5, 1993, pp. 1141-1158

[8] Kim, S.-G., Tahk, M.-J., "Output-Redefinition Based on Robust Zero Dynamics," *Proceedings of the AIAA Guidance, Navigation, and Control Conference*, AIAA Paper 98-4493, 1998.

[9] Albus, J.S., "A New Approach to Manipulator Control: The Cerebellar Model Articulation Controller (CMAC)", *Transactions of the ASME, Journal on Dynamics Systems, Measurement and Control*, Vol. 97, No. 3, 1975, pp. 220-227.

[10] Smith, R., *Intelligent Motion Control with an Artificial Cerebellum*, PhD-Thesis, Department of Electrical and Electronic Engineering, University of Auckland, New Zealand, July 1998.

[11] Wallner, E., "Nonlinear and Neural Adaptive Approaches to Flight Control Problems: X-38 and X-31", Dissertation, Institute for Flight Mechanics and Control, University of Stuttgart, 2004.